Characterization of low frequency instabilities in a Krypton dusty plasma

Hagop Tawidian, Thomas Lecas, Maxime Mikikian

Characterization of low frequency instabilities in a Krypton dusty plasma

H. Tawidian, T. Lecas, and M. Mikikian

GREMI, Groupe de Recherches sur l'Energétique des Milieux Ionisés, UMR7344 CNRS/Univ. Orléans, F-45067 Orléans, France

E-mail: maxime.mikikian@univ-orleans.fr

Abstract. The occurrence of low frequency instabilities in a plasma can be due to the presence of a high density of grown dust particles. These instabilities are characterized by analyzing the discharge current, evidencing the existence of successive phases marked by distinct frequency evolutions. The main characteristics of these phases are determined as a function of the gas pressure. A particular attention is paid to the changes of the instability appearance time, duration and frequencies. These parameters seem to be related with the global amount of grown dust particles. The instability appearance time is the first parameter that can be easily measured during an experiment and all the other parameters can be estimated from this simple measurement.

PACS numbers: 52.27.Lw, 52.35.-g

Submitted to: *Plasma Sources Sci. Technol.*

1. Introduction

In addition to the neutral species, dusty plasmas [1] are constituted of three charged components: ions, electrons and bigger particles called dust particles. The size of these solid particles can vary from a few nanometers to millimeters. In astrophysics, dusty plasmas can be observed for example in comets tails or in some planetary atmospheres [2, 3]. In industry, the formation of dust particles was observed in plasma processing reactors in the late 80s [4]. Their appearance was an unexpected problem in the field of microelectronics where cleanliness is a drastic requirement for the fabrication process of semiconductors. Several techniques [5, 6, 7, 8, 9] were then proposed to remove them away from the processed surfaces. In fusion reactors like ITER, the presence of dust particles remains a critical issue [10, 11]. Whereas these nano sized particles are harmful in many processes, nowadays they are also considered for several applications like solar cells [12] and memories. In laboratories, dust particles can be easily grown using several methods like reactive gases [13, 14, 15, 16, 17, 18, 19, 20, 21] or material sputtering [22, 23, 24, 25, 26]. Thanks to these methods, molecular precursors are created in the discharge and are at the origin of chemical reactions leading to the growth of dust particles. As soon as these particles reach a sufficient size, they acquire a negative charge by capturing plasma electrons. This loss of electrons can lead to modifications in the plasma characteristics [27, 28, 29] and when the dust particle density is huge, different types of low frequency (from a few to a few hundreds Hz) instabilities can be observed: dust particle growth instabilities [22, 23, 30, 31] including plasmoids [32, 33, 34, 35], successive generation instabilities [18, 36, 37] and the heartbeat instability [38, 39, 40, 41]. Some plasma instabilities (MHz range) related to dust particle growth can also be observed in electron cyclotron resonance plasmas [42].

The present study is mainly focused on the analysis of dust particle growth instabilities (DPGI). The so-called DPGI, detailed in Sec. 3, is investigated by recording the discharge current during dust particle growth obtained by material sputtering. This signal reveals the temporal evolution of the instability. A Fourier analysis shows the existence of different instability regimes and complex frequency evolutions (Sec. 4). An alternation of ordered and stochastic regimes is evidenced. The ordered regimes are characterized by a well-defined frequency value that evolves smoothly as a function of time. On the contrary, during the stochastic regime the frequency is changing very quickly and erratically around a mean value. The evolution of these regimes is studied as a function of the gas pressure (Sec. 5) and some instability characteristics (appearance time, duration, typical frequencies) are compared. It appears that the simple measurement during an experiment of the instability appearance time is a good indication of the entire instability evolution (Sec. 6). The experimental results are discussed in Sec. 7.

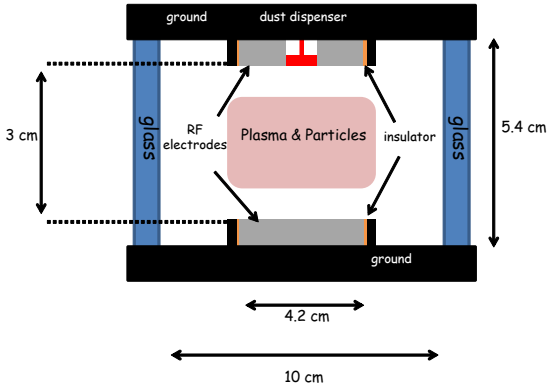

Figure 1. Scheme of the PKE-Nefedov reactor.

2. Experimental setup

The experiments are performed in the PKE-Nefedov [43] reactor where the plasma is created by a capacitively coupled radio-frequency (13.56 MHz in push-pull mode) discharge with a typical power of 3 W. The two parallel electrodes (4.2 cm in diameter, separated by 3 cm) are surrounded by guard rings (figure 1). Dust particles are grown in the plasma by sputtering previously injected micrometer size dust particles made of polymer (melamine formaldehyde) and lying on the electrodes [24]. After each experiment, the grown dust particles fall down on the bottom electrode and this deposition is also sputtered during the experiments. Krypton is used as the sputtering gas with a typical pressure between 1.4 and 2.4 mbar. The growth process is highly sensitive to gas purity, and this effect can be amplified by the fact that experiments are performed without continuous gas flow. Before each experiment, the gas line and the reactor are pumped down to a low base pressure of 10^{-6} mbar in order to eliminate the molecular impurities from the previous experiment. This pumping method is favorable to form a high dust particle density and to obtain relatively reproducible results [23, 24]. For each studied pressure, several experiments are performed in order to obtain statistical measurements and estimate error bars.

3. Dust particle growth instabilities

Once the plasma is switched on, the dust particle growth process starts. This growth is easily identified by measuring the temporal evolution of the amplitude of the discharge current fundamental harmonic (DC component, figure 2). Indeed, as dust particles are growing, they attach more and more free electrons. It results in the global decrease of the discharge current [9]. After a few tens of seconds, dust particles strongly disturb the plasma equilibrium and DPGI start. They are easily detected in figure 2 and correspond to an increase of the signal fluctuation around its mean value. During DPGI, the plasma is highly unstable and shows very complex structure and behaviour [34]. While dust particles were easily observed in the Ar case [30], they are hardly visible with Kr. Our

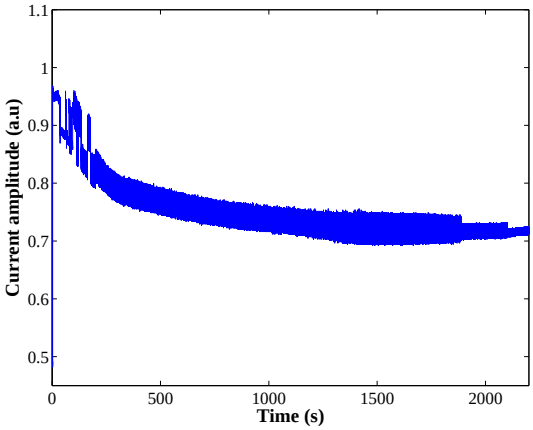

Figure 2. Amplitude of the rf current (DC component) as a function of time.

visual observations (at the extinction of the plasma thanks to laser light scattering) tend to show that the use of Kr leads to the formation of a denser cloud of smaller dust particles. When the plasma is turned off, the dust cloud is more easily observed as the oscillating plasma glow is no more disturbing the observation. In addition, dust particles are very light and immersed in a neutral gas at rest (static pressure) and at a relatively high pressure. Thus, the dust cloud falling can take several seconds due to the small gravitational force and the non negligible friction with the neutral gas. It is then possible to observe the dust cloud more easily than during the plasma ON phase. No clear void is detected in the center of the dust cloud and DPGI appear during the growth of a single dust particle generation. In the presented experiments, as the void does not appear, no cyclic formation of dust particles is obtained [13, 18, 21, 44, 45]. It is confirmed by figure 2 where no very low-frequency oscillations of the signal (period of a few minutes) is detected.

Some sudden amplitude drops in the electrical signal are noticed when using Kr. These drops last for a few seconds and are evidenced just after the plasma ignition and during the first part of the instabilities as clearly observed in figure 2. Later in the growth process, the existence of these drops is no more evidenced. They are also not obtained without dust particle growth. For these reasons, we do not attribute these drops to any problem in the electrical wiring circuit. Their origin is currently under investigation and their connection with dust particle growth is considered.

4. Evidence of different instability regimes

In figure 3, the AC part of the discharge current is recorded from the plasma ignition till its extinction at a pressure of 1.8 mbar. Measuring the AC component gives a much higher resolution than the DC component (figure 2) for analyzing the DPGI frequency evolution. The plasma ignition is detected as a sharp peak 3 s after the recording start (due to the time scale used in figure 3, it is superimposed on the y-axis). The instability begins several tens of seconds after the plasma ignition and

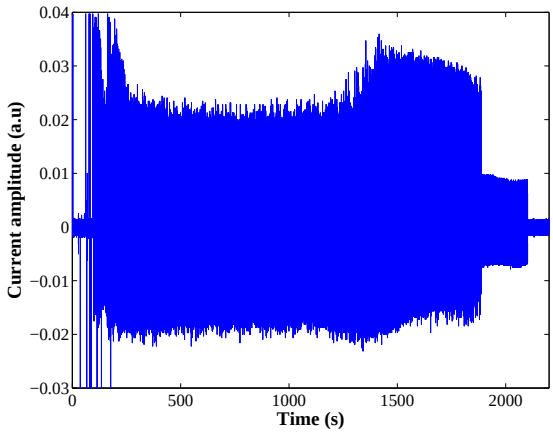

Figure 3. Alternative part of the discharge current amplitude evidencing DPGI.

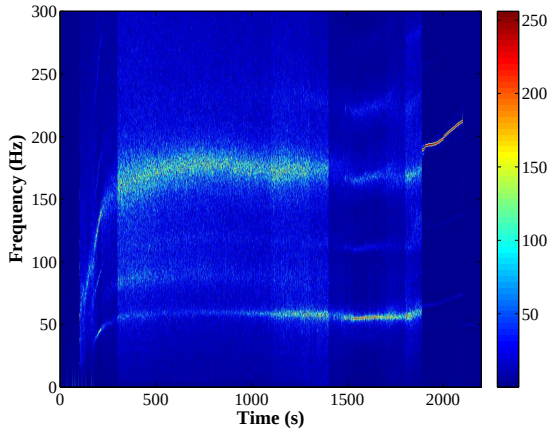

Figure 4. Fourier spectrogram of the electrical measurements shown in figure 3 and representing the frequency evolution of DPGI.

lasts about 2000 s. The DPGI frequency evolution is evidenced by calculating the corresponding Fourier spectrogram (figure 4). In order to emphasize small ordered domains, the spectrogram intensity has been normalized separately inside each 100 s range [30] (from 0 to 100 s the intensity has been normalized to its maximum value inside this time domain and so on). From figures 3 and 4, it clearly appears that the instability is characterized by a well defined succession of phases. These phases can be either ordered with a smoothly evolving frequency, or stochastic with fast and erratic frequency variations. In figure 4, the main stochastic phase clearly appears between 400 and 1300 s. These phases are also well identified in figure 3 where they are characterized by different instability amplitudes. In figure 4, when several frequencies are detected simultaneously, the colour code allows to identify the dominant frequency. Indeed, the electrical measurements show that the instability is constituted of well defined patterns with a varying number of peaks. Depending on the respective peak amplitudes, the dominant frequency corresponds either to the main frequency pattern (constituted of several peaks) or to the peak separation within the pattern [35].

At the beginning of the instability, a fast increase of the frequency is observed until 400 s (figure 4). During this period, the instability alternates between ordered and more stochastic phases. Then, a long stochastic phase starts at 400 s up to 1300 s. The frequency fluctuates around 170 Hz quickly and erratically but stays within a rather small value range. During this period, the envelope amplitude of the electrical signal stays roughly at the same height (figure 3) and the most highlighted frequency (figure 4) corresponds to the frequency between consecutive peaks. During this phase no specific pattern can be determined due to the stochastic evolution. Then, the frequency decreases to about 55 Hz at around 1300 s. This change appears as an increase of the signal amplitude in figure 3, and to the appearance of a clear two peak pattern, the dominant frequency being the main pattern frequency (and not the frequency corresponding to the two peak separation). Finally, the instability ends with an ordered phase characterized by a high frequency ($\simeq$ 200 Hz in figure 4) and a small amplitude (figure 3).

In this section, we have briefly identified different phases and showed a complex evolution of the main frequency. In order to better understand the instability behaviour, its modification as a function of the pressure is now investigated.

5. Pressure dependence of DPGI

The evolution of the RF current amplitude (DC component) as a function of time is presented for different pressures from 1.4 to 2.4 mbar in figure 5. At the plasma ignition, it is observed that the higher the pressure, the higher the rise of the signal. Then, the current decrease due to dust particle growth is slightly different as a function of the pressure. For instance, at 1.4 and 1.6 mbar, the decrease is slow and the amplitude variation is small. At 1.8 mbar, the current decrease becomes faster and a clear gap can be observed between the curves at 1.6 and 1.8 mbar. At 2 and 2.4 mbar, the current decrease continues to accelerate. The gap observed between 2 mbar and 2.4 mbar could be the place of a missing measurement at 2.2 mbar (not available due to experimental problems during the measurement campaign). These measurements show that at higher pressures (above 1.6 mbar) the growth kinetics is faster and the dust density is higher (the bigger is the amount of formed dust particles, the bigger is the loss of electrons). These hypotheses are consistent with the visual observation of the dust cloud falling at the extinction of the plasma (the dust cloud is hardly visible by laser light scattering during the plasma phase due to the small dust particle size).

In the same range of pressures (from 1.4 to 2.4 mbar), the instability characteristics are determined. The evolution of the appearance time and total duration of DPGI are presented in figure 6. Error bars are estimated from a statistics based on several experiments performed in the same conditions. A long pumping period (at least one half-day) between each experiment guarantees that the amount of impurities (strongly affecting the dust particle growth process) is low and rather similar for each experiment. At 1.4 mbar, the instability appears around 220 s after the plasma ignition, while at

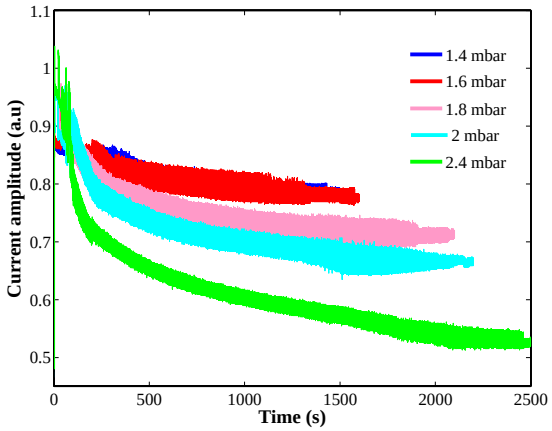

Figure 5. Amplitude of the rf current (DC component) as a function of time for different pressures.

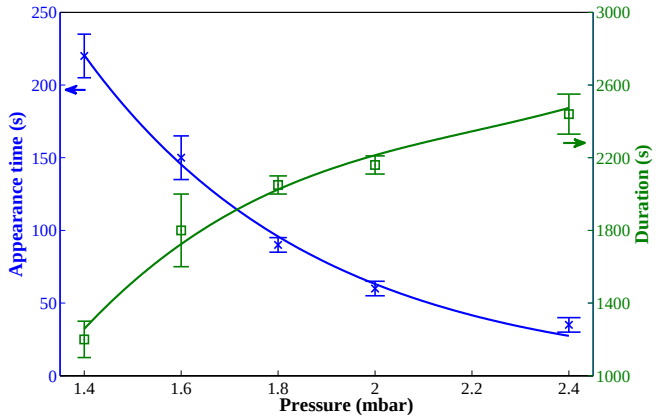

Figure 6. Appearance time (×) and total duration (□) of DPGI as a function of the gas pressure.

2.4 mbar it occurs more quickly (35 s). Increasing the pressure results in a continuous decrease of the appearance time that can be easily fitted by a decreasing exponential function. It means that the necessary conditions to trigger DPGI are obtained faster at high pressure. Anew, it is consistent with the observation that higher pressures result in the growth of a higher dust density (and thus smaller dust sizes) as shown in figure 5. These conditions seem to be more favorable to trigger DPGI than situations with a lower density of bigger dust particles obtained at low pressures [30].

Concerning the instability duration, it increases with the pressure from 1200 s at 1.4 mbar up to 2400 s at 2.4 mbar. The duration trend can also be fitted by an exponential function in the form $a - b.exp(-c.P)$. At high pressures, the amount of dust particles is large enough to sustain the instability for a long duration. From the behaviours observed in figure 6, it can be deduced that the higher the pressure, the shorter the appearance time and the longer the duration of the instability. Thus, a high dust particle density is required to induce well developed instabilities. During experiments, this observation can provide an easy indication of the amount of grown dust particles.

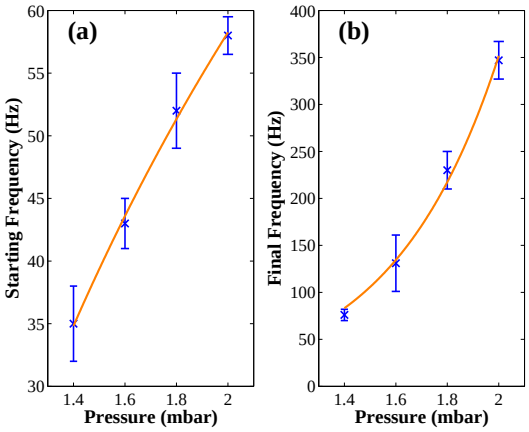

Figure 7. (a) Starting and (b) final frequencies of the instability as a function of the pressure.

Dust particle growth kinetics can also be estimated from the evolution of the DPGI frequency. For this purpose, the starting (at the instability beginning) and final (just before the instability end) frequencies are measured as a function of the pressure (figure 7). At 1.4 mbar, the starting frequency is around 35 Hz and it increases with the pressure up to a value of about 58 Hz at 2 mbar (an increase of 1.6 times). The final frequency is around 75 Hz at 1.4 mbar, and it increases with the pressure up to 350 Hz at 2 mbar (an increase of 4.6 times). The ratio between the final and starting frequencies is also highly dependent on the pressure, from a factor 2 at 1.4 mbar, 3 at 1.6 mbar, 4.5 at 1.8 mbar and 6 at 2 mbar. At 2.4 mbar, the signal is mostly dominated by a stochastic behaviour, and thus starting and final frequencies cannot be clearly defined. A relatively small difference in the starting frequency can thus result in rather different final frequencies confirming the pressure dependence of dust particle growth kinetics. In order to better investigate the frequency evolution during dust particle growth, the four main phases of DPGI (figure 4) are analyzed as a function of the gas pressure. As shown in section 4, these successive phases are:

- From the beginning up to the main stochastic regime (till 400 s). The evolution of the frequency during this period is discussed in [35].
- The main central stochastic regime (from 400 s up to around 1300 s).
- The frequency drop phase.
- The last ordered phase (around 2000 s).

In figure 8, the first part of the instability is observed for four values of the pressure (1.4, 1.6, 1.8, and 2 mbar). For a better comparison, the same time and frequency scales are used for each pressure. Some conclusions drawn from figures 6 and 7 (on the appearance time and starting frequencies) can also be found again in this figure. At 1.4 mbar, several ordered phases are observed at the beginning of the instability before the long stochastic phase. The frequency increases slowly with a speed of about 0.07 Hz/s. At 1.6 mbar, the first part of the instability becomes shorter and an alternation of ordered and stochastic behaviour is observed before the beginning of the long stochastic

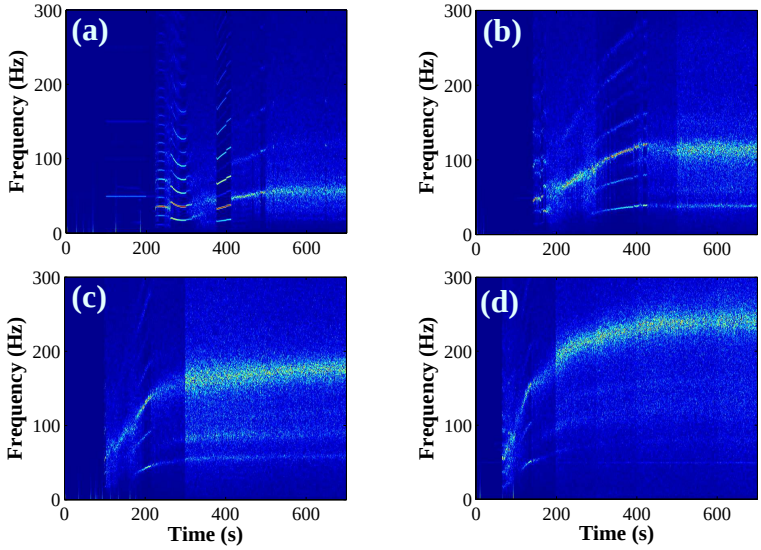

Figure 8. Fourier spectrogram of the first phases for different pressures, (a) 1.4 mbar, (b) 1.6 mbar, (c) 1.8 mbar and (d) 2 mbar.

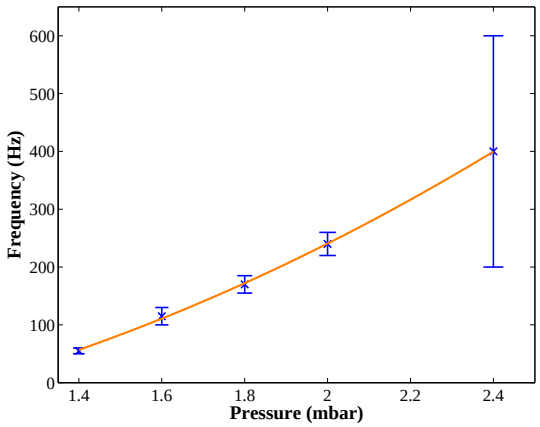

Figure 9. Central stochastic phase frequency as a function of the pressure.

phase at around 500 s. During this first part, the frequency increases with a speed of about 0.25 Hz/s. At 1.8 mbar, the rise of the frequency is faster with a speed of 0.5 Hz/s, and the first part of the instability becomes mostly stochastic. At 2 mbar, the first part of the instability is brief and the frequency increases at a speed of 0.9 Hz/s. These evolutions show that at high pressure, the frequency increases faster than at low pressure and is related to the formation of a high dust density.

The first phases of the instability are followed by the main stochastic regime, a relatively robust phase appearing during all our experiments. In figure 9, the long stochastic phase frequency is shown as a function of the pressure. The frequency mean value is around 55 Hz at 1.4 mbar, and increases up to 240 Hz at 2 mbar. At 2.4 mbar, this frequency can strongly vary from one experiment to another. It is mainly due to the strong stochastic behaviour of DPGI at pressures above 2 mbar as already mentioned

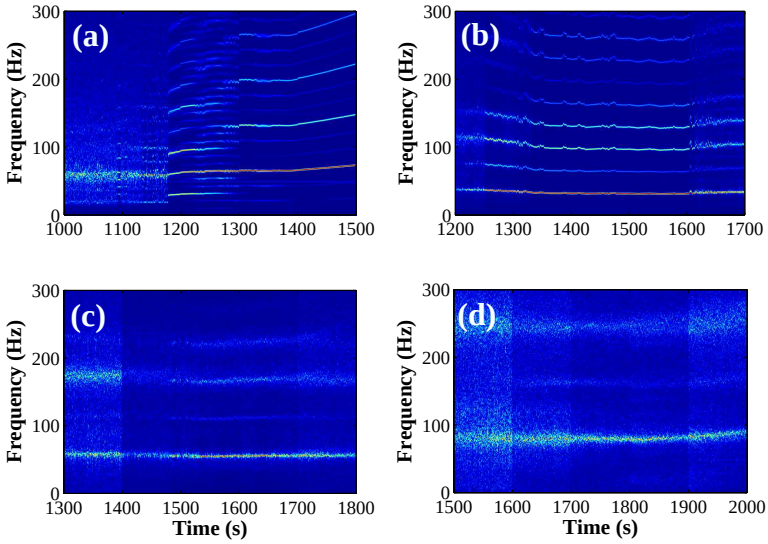

Figure 10. Fourier spectrogram of the frequency drop phase for different pressures, (a) 1.4 mbar, (b) 1.6 mbar, (c) 1.8 and (d) 2 mbar.

for figure 7. Indeed, in our experimental conditions these pressures lead to very strong stochastic instabilities that can evolve quite differently. Nevertheless, as we performed many experiments for each pressure, we found that the average frequency at 2.4 mbar fit rather well with the global trend as function of the pressure. Thus, we can conclude that as for the starting and final frequencies (figure 7), the central stochastic frequency also increases with the pressure.

After this long stochastic phase, the frequency decreases to a smaller value (figure 10 (a) 1.4, (b) 1.6, (c) 1.8 and (d) 2 mbar). This is mainly due to the fact that for this phase, the frequency corresponds to the pattern frequency and no more to the consecutive peak frequency. This phase is constituted of two parts, a well-ordered one and a more stochastic one. As expected, this phase is more ordered at low pressure. At 1.4 mbar, it begins around 1180 s (figure 10 (a)) where a frequency at 32 Hz and its harmonics are observed for a short time until 1220 s, then the frequency at 65 Hz becomes dominant. At 1.6 mbar, the phase is clearly evidenced around 1250 till 1600 s (figure 10 (b)) before turning into a more stochastic behaviour. At 1.8 mbar (figure 10 (c)), it is globally more stochastic, meaning that a pattern exists but it is disturbed by the appearance of random peaks. Finally at pressures above 2 mbar, the stochastic behaviour is completely dominant and at 2.4 mbar this phase is the final one before the end of the instability: the last ordered phase (figure 4) is not observed.

At pressures lower than 2.4 mbar, another phase occurs before the instability end. This final phase has a clear ordered behaviour as shown in figure 11. At high pressure, the phase is shorter than at low pressure, and the shape of the frequency evolution is different. At 1.4 mbar, the frequency increases slowly with a speed of about 0.09 Hz/s then slightly decreases at the end. At 1.6 mbar, the frequency increases with a speed of 0.10 Hz/s and the last decrease is less marked. At 1.8 mbar, the speed is around 0.13

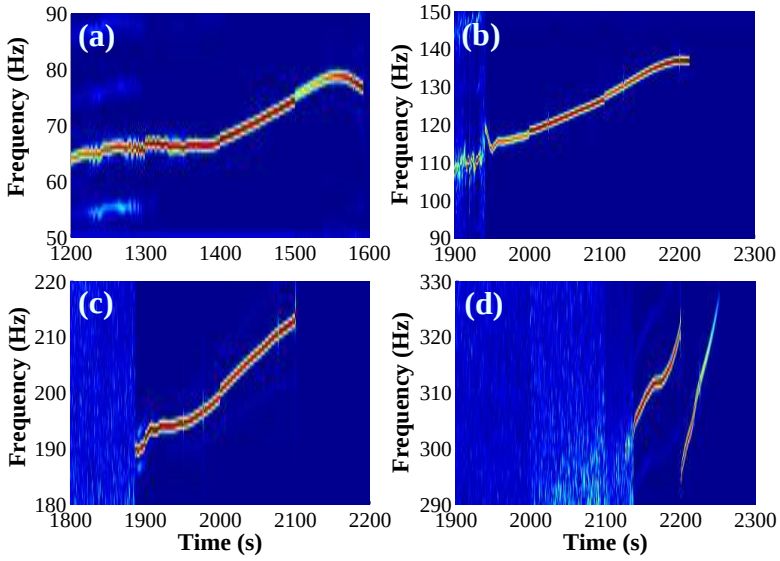

Figure 11. Spectrogram of the last ordered phase before the end of the instabilities, (a) at 1.4 mbar, (b) 1.6 mbar, (c) 1.8 mbar and (d) 2 mbar.

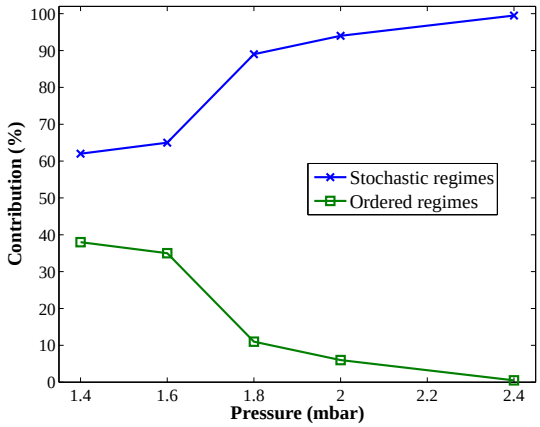

Figure 12. Contribution of the ordered (□) and stochastic (×) regimes as a function of the pressure.

Hz/s and the last decrease is not observed. At 2 mbar, this phase is divided into two parts, with a rising speed of about 0.63 Hz/s. The frequency evolution becomes faster as a function of the pressure as we already observed at the beginning of the instability (figure 8). In figure 11, it clearly appears that the duration of this ordered phase decreases with the pressure. The splitting of this phase at 2 mbar is a first indication of the weakness of the ordered behaviours at high pressure. It is a sign of the future disappearance of this phase at 2.4 mbar.

The progressive disappearance of the ordered phases at high pressure is clearly evidenced in figure 12. In this figure, the relative contributions of the ordered and stochastic phases have been measured. The durations of all the stochastic phases occurring during a DPGI sequence have been summed up. The same procedure has

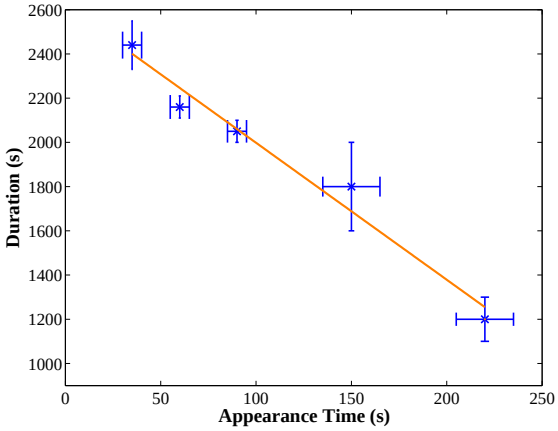

Figure 13. Duration of the entire instability as a function of the appearance time.

been used for the ordered regimes. At 1.4 mbar, the two types of phases have roughly the same duration, whereas the stochastic phases become dominant as the pressure is increased. At 2.4 mbar, the ordered phases are almost absent, and DPGI are mainly stochastic during their whole duration. It means that when the dust particle density is huge (and thus the dust particle size is small), the instability cannot enter in an ordered regime. The disturbance induced by the dust particles is too strong to allow the instability to have an ordered oscillating behaviour.

6. Interdependency between instability parameters

In the previous section, the evolution of the instability characteristics has been studied as a function of the pressure. In the present section, relations between these different characteristics is emphasized. During an experiment, the first parameter that can be easily measured is the instability appearance time. The knowledge of this single parameter provides information on the instability evolution. In figure 13, the instability duration is plotted as a function of the appearance time. It clearly shows the result of figure 6 that the longer the appearance time, the shorter the instability duration. When the instability appears 35 s after the plasma ignition, it can last for 2400 s. When it starts 220 s after the plasma ignition, the total duration of the instability is only 1200 s. Figure 13 shows that there is roughly an inversely linear dependence between the instability duration and appearance time. The duration of DPGI can thus be roughly predicted as soon as they appear. Thanks to the appearance time, the different frequencies of the instability (starting, during the long stochastic phase, and final) can also be determined as shown in figure 14 (the evolution of the starting frequency is zoomed in the upper right insert). The frequency trends have been fitted by decreasing exponential functions. Figure 14 clearly shows the relation between the frequencies discussed previously in figure 7. A quick start of the instability (60 s after plasma ignition) shows a strong temporal increase of the mean frequency (a factor of 6 between the starting and the final frequencies). For a longer appearance time (220 s

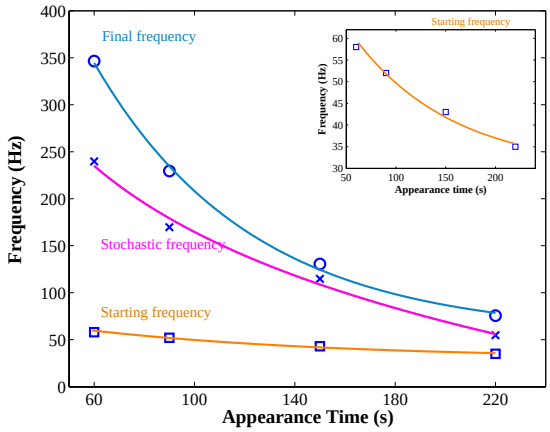

Figure 14. Starting (□), stochastic (×), and final (○) frequencies of the instability as a function of the appearance time.

after plasma ignition), the factor between the starting and the final frequencies becomes only 2. It means that the earlier is the appearance of the instability, the bigger is the global increase of the frequency.

These dependences with the appearance time show that DPGI is a relatively robust phenomenon and that small fluctuations in the starting conditions do not change its long term evolution. This conclusion has to be slightly moderated for the high pressures. It can be useful for the experimenters, as the knowledge of the appearance time is enough to know rather accurately the instability evolution.

7. Discussion and Conclusions

In this paper, we characterized instabilities triggered by the presence of a high density of grown dust particles in a Kr plasma. These instabilities are analyzed using electrical measurements: the amplitude of the discharge current is recorded from the ignition till the extinction of the plasma. The Fourier spectrogram brings to light the temporal evolution of the frequencies during the instability. In particular, a succession of different ordered and stochastic phases are identified as in the Ar case [30]. The differences between the two gases mainly concerns the frequency values and evolution within the phases. Frequencies are higher in Kr certainly due to a higher dust particle density and a smaller dust particle size. A systematic comparison between the two gases has to be performed with experiments completely dedicated to this defined study. In this paper we focused our analysis on the measurement of the instability characteristics as a function of the Kr pressure. It appears that the higher the pressure, the shorter the appearance time (figure 6), the longer the duration (figure 6) and the higher the frequencies (figures 7 and 9). These results are consistent with the observation performed in figure 5, that at high pressure the decrease of the current amplitude is sharper. It means that the growth kinetics is faster [24, 46] and the dust density is certainly higher (usually connected with a smaller dust particle size [30]). Indeed, our experimental observations tend to

show that a fast growth kinetics and a high dust density lead to a rapid appearance of DPGI. As the disturbance is strong and the discharge is saturated by dust particles, the instability can thus last longer. For the frequencies, a direct correlation is more difficult to define. Indeed, a simple approximation consists in considering that the typical DPGI frequencies are related to the dust plasma frequency [1, 9, 47] $\omega_{pd} = \sqrt{\frac{Q_d^2 n_d}{\epsilon_0 m_d}} \propto \sqrt{\frac{n_d}{r_d}}$ (where n_d is the dust density, Q_d the dust charge, m_d the dust mass and r_d the dust radius). As n_d is higher and r_d is smaller at high pressure, it is logical to obtain a global increase of the typical DPGI frequencies with the pressure (figures 7 and 9). Nevertheless, this simple consideration cannot clearly explain the frequency temporal evolution. Whereas, the frequency increase at the beginning (figure 8) could be related to an increase of n_d due to the sputtering process, the stochastic phase and the last ordered phase cannot be easily related to ω_{pd}. In the long stochastic phase, the mean frequency is relatively constant. It is not consistent with growing dust particles. An hypothesis can be that we have a slowing down of the dust particle growth during this regime, and then, rather constant values of n_d and r_d. The last ordered phase is characterized by a frequency increase. As n_d is not expected to increase at this stage of the dust particle growth process (no indication of a new dust particle generation is observed) the relation with ω_{pd} is rather difficult. This behaviour shows that more complex phenomena are driving DPGI and further investigations need to be conducted to analyze the evolution of dust and plasma properties. For example, the use of in-situ diagnostics like ellipsometry [21, 45] will give access to dust particle size and will allow a better correlation with DPGI evolution. Finally, we emphasized that the single measurement of the appearance time provides an estimation of the other instability properties thanks to linear and exponential dependences. It can be an easy and useful indication for the experimenter as soon as the instability begins. In the future, the evolution of the instability amplitude will be also further investigated. Indeed, as shown in figure 3, the amplitude variations could be connected to dust particle growth dynamics.

Acknowledgments

The PKE-Nefedov chamber has been made available by the Max-Planck-Institute for Extraterrestrial Physics, Germany, under the funding of DLR/BMBF under Grant No. 50WM9852. This work was supported by the French National Research Agency (ANR), project INDIGO n° ANR-11-JS09-010-01

References

[1] P. K. Shukla and B. Eliasson. Colloquium: Fundamentals of dust-plasma interactions. *Rev. Mod. Phys.*, 81:25, 2009.

[2] E. Kovačević, I. Stefanović, J. Berndt, Y. J. Pendleton, and J. Winter. A candidate analog for carbonaceous interstellar dust: Formation by reactive plasma polymerization. *ApJ*, 623:242, 2005.

[3] E. Sciamma-O'Brien, P.R. Dahoo, E. Hadamcik, N. Carrasco, E. Quirico, C. Szopa, and G. Cernogora. Optical constants from 370 nm to 900 nm of titan tholins produced in a low pressure rf plasma discharge. *Icarus*, 218:356, 2012.

[4] G. S. Selwyn, J. Singh, and R. S. Bennett. In situ laser diagnostic studies of plasma generated particulate contamination. *J. Vac. Sci. Technol. A*, 7:2758, 1989.

[5] Y. Kurimoto, N. Matsuda, G. Uchida, S. Iizuka, M. Suemitsu, and N. Sato. Fine particle removal by a negatively-charged fine particle collector in silane plasma. *Thin Solid Films*, 457:285, 2004.

[6] S. Iizuka, K. Sakuta, W. Suzukawa, K. Kato, and T. Gohda. Control of fine particles by time-averaged external forces in plasmas. *Phys. Plasmas*, 13:103502, 2006.

[7] Y.-F. Li, U. Konopka, K. Jiang, T. Shimizu, H. Höfner, H. M. Thomas, and G.E. Morfill. Removing dust particles from a large area discharge. *Appl. Phys. Lett.*, 94:081502, 2009.

[8] C. M. Ticos, I. Jepu, C. P. Lungu, P. Chiru, V. Zaroschi, and A. M. Lungu. Removal of floating dust in glow discharge using plasma jet. *Appl. Phys. Lett.*, 97:011501, 2010.

[9] M. Mikikian, L. Couëdel, M. Cavarroc, Y. Tessier, and L. Boufendi. Dusty plasmas: synthesis, structure and dynamics of a dust cloud in a plasma. *Eur. Phys. J. Appl. Phys.*, 49:13106, 2010.

[10] S I Krasheninnikov, A Yu Pigarov, R D Smirnov, M Rosenberg, Y Tanaka, D J Benson, T K Soboleva, T D Rognlien, D A Mendis, B D Bray, D L Rudakov, J H Yu, W P West, A L Roquemore, C H Skinner, J L Terry, B Lipschultz, A Bader, R S Granetz, C S Pitcher, N Ohno, S Takamura, S Masuzaki, N Ashikawa, M Shiratani, M Tokitani, R Kumazawa, N Asakura, T Nakano, A M Litnovsky, R Maqueda, and the LHD Experimental Group. Recent progress in understanding the behavior of dust in fusion devices. *Plasma Phys. Control. Fusion*, 50:124054, 2008.

[11] C. Arnas, C. Pardanaud, C. Martin, P. Roubin, G. De Temmerman, and G. Counsell. Analyses of dust samples collected in the mast tokamak. *J. Nucl. Mater.*, 401:130, 2010.

[12] P. Roca i Cabarrocas, R. Cariou, and M. Labrune. Low temperature plasma deposition of silicon thin films: From amorphous to crystalline. *J. Non-Cryst. Solids*, 358:2000, 2012.

[13] J. Berndt, E. Kovačević, I. Stefanović, O. Stepanovic, S. H. Hong, L. Boufendi, and J. Winter. Some aspects of reactive complex plasmas. *Contrib. Plasma Phys.*, 49:107, 2009.

[14] K. De Bleecker, A. Bogaerts, and W. Goedheer. Detailed modeling of hydrocarbon nanoparticle nucleation in acetylene discharges. *Phys. Rev. E*, 73:026405, 2006.

[15] M. Hundt, P. Sadler, I. Levchenko, M. Wolter, H. Kersten, and K. Ostrikov. Real-time monitoring of nucleation-growth cycle of carbon nanoparticles in acetylene plasmas. *J. Appl. Phys.*, 109:123305, 2011.

[16] M. Calafat, P. Yuryev, A. Drenik, A. Slim, and R. Clergereaux. Carbon Nanoparticle/Hydrogenated amorphous carbon composite thin films formed in ECR plasma. *Plasma Process. Polym.*, 8:401, 2011.

[17] I. Géraud-Grenier, R. Jaffiol, V. Massereau-Guilbaud, and A. Plain. Photoluminescence of hydrogen amorphous carbon nitrile particles obtained in a 13.56 MHz dusty plasma. *Appl. Phys. Lett.*, 99:091503, 2011.

[18] B. Despax, K. Makasheva, and H. Caquineau. Cyclic powder formation during pulsed injection of hexamethyldisiloxane in an axially asymmetric radiofrequency argon discharge. *J. Appl. Phys.*, 112:093302, 2012.

[19] V. Massereau-Guilbaud, I. Géraud-Grenier, J. F. Lagrange, H. Tawidian, and M. Mikikian. Electron temperature evolution in a low pressure dusty rf nitrogen-rich methane plasma. *IEEE Trans. Plasma Sci.*, 41:816, 2013.

[20] M. Schulze, A. von Keudell, and P. Awakowicz. Controlled particle generation in an inductively coupled plasma. *Appl. Phys. Lett.*, 88:141503, 2006.

[21] F. Greiner, J. Carstensen, N. Kohler, I. Pilch, H. Ketelsen, S. Knist, and A. Piel. Imaging Mie ellipsometry: dynamics of nanodust clouds in an argon-acetylene plasma. *Plasma Sources Sci. Technol.*, 21:065005, 2012.

[22] G. Praburam and J. Goree. Experimental observation of very low-frequency macroscopic modes

in a dusty plasma. *Phys. Plasmas*, 3:1212, 1996.

[23] D. Samsonov and J. Goree. Instabilities in a dusty plasma with ion drag and ionization. *Phys. Rev. E*, 59:1047, 1999.

[24] M. Mikikian, L. Boufendi, A. Bouchoule, H. M. Thomas, G. E. Morfill, A. P. Nefedov, V. E. Fortov, and the PKE-Nefedov Team. Formation and behaviour of dust particle clouds in a radio-frequency discharge: results in the laboratory and under microgravity conditions. *New J. Phys.*, 5:19, 2003.

[25] C. Arnas and A. A. Mouberi. Thermal balance of carbon nanoparticles in sputtering discharges. *J. Appl. Phys.*, 105:063301, 2009.

[26] A. Michau, G. Lombardi, L.C. Delacqua, M. Redolfi, C. Arnas, P. Jestin, X. Bonnin, and K. Hassouni. Field reversal and particle growth in dc discharge. *Plasma Chem. Plasma Process*, 32:451, 2012.

[27] I. Goertz, F. Greiner, and A. Piel. Effects of charge depletion in dusty plasmas. *Phys. Plasmas*, 18:013703, 2011.

[28] S. Hübner and A. Melzer. Dust-induced modulation of the atomic emission in a dusty argon discharge. *Phys. Rev. Lett.*, 102:215001, 2009.

[29] S. Mitic, M. Y. Pustylnik, and G. E. Morfill. Spectroscopic evaluation of the effect of the microparticles on radiofrequency argon plasma. *New J. Phys.*, 11:083020, 2009.

[30] M. Mikikian, M. Cavarroc, L. Couëdel, and L. Boufendi. Low frequency instabilities during dust particle growth in a radio-frequency plasma. *Phys. Plasmas*, 13:092103, 2006.

[31] M. Mikikian, L. Couëdel, M. Cavarroc, Y. Tessier, and L. Boufendi. Plasma emission modifications and instabilities induced by the presence of growing dust particles. *IEEE Trans. Plasma Sci.*, 36:1012, 2008.

[32] M. Mikikian, L. Couëdel, Y. Tessier, and L. Boufendi. Carousel instability in a capacitively-coupled RF dusty plasma. *IEEE Trans. Plasma Sci.*, 39:2748, 2011.

[33] H. Tawidian, M. Mikikian, L. Couëdel, and T. Lecas. Plasma inhomogeneities near the electrodes of a capacitively-coupled radio-frequency discharge containing dust particles. *Eur. Phys. J. Appl. Phys.*, 56:24018, 2011.

[34] M. Mikikian, H. Tawidian, and T. Lecas. Merging and splitting of plasma spheroids in a dusty plasma. *Phys. Rev. Lett.*, 109:254007, 2012.

[35] H. Tawidian, T. Lecas, and M. Mikikian. Zoom into dusty plasma instabilities. *IEEE Trans. Plasma Sci.*, 41:754, 2013.

[36] M. Cavarroc, M. Mikikian, Y. Tessier, and L. Boufendi. Instabilities during the growth of dust successive generations in silane-based plasmas. *Phys. Plasmas*, 15:103704, 2008.

[37] L. Couëdel, M. Mikikian, A. A. Samarian, and L. Boufendi. Self-excited void instability during dust particle growth in a dusty plasma. *Phys. Plasmas*, 17:083705, 2010.

[38] M. Mikikian, M. Cavarroc, L. Couëdel, Y. Tessier, and L. Boufendi. Mixed mode oscillations in complex plasma instabilities. *Phys. Rev. Lett.*, 100:225005, 2008.

[39] M. Mikikian, L. Couëdel, M. Cavarroc, Y. Tessier, and L. Boufendi. Threshold phenomena in a throbbing complex plasma. *Phys. Rev. Lett.*, 105:075002, 2010.

[40] M. Y. Pustylnik, A. V. Ivlev, N. Sadeghi, R. Heidemann, S. Mitic, H. M. Thomas, and G. E. Morfill. On the heterogeneous character of the heartbeat instability in complex (dusty) plasmas. *Phys. Plasmas*, 19:103701, 2012.

[41] R. J. Heidemann, L. Couëdel, S. K. Zhdanov, K. R. Sütterlin, M. Schwabe, H. M. Thomas, A. V. Ivlev, T. Hagl, G. E. Morfill, V. E. Fortov, V. I. Molotkov, O. F. Petrov, A. I. Lipaev, V. Tokarev, T. Reiter, and P. Vinogradov. Comprehensive experimental study of heartbeat oscillations observed under microgravity conditions in the PK-3 plus laboratory on board the international space station. *Phys. Plasmas*, 18:053701, 2011.

[42] A. Drenik, P. Yuryev, A. Vesel, J. Margot, and R. Clergereaux. Observation of plasma instabilities related to dust particle growth mechanisms in electron cyclotron resonance plasmas. *Phys. Plasmas*, 20:100701, 2013.

[43] A. P. Nefedov, G. E. Morfill, V. E. Fortov, H. M. Thomas, H. Rothermel, T. Hagl, A. Ivlev, M. Zuzic, B. A. Klumov, A. M. Lipaev, V. I. Molotkov, O. F. Petrov, Y. P. Gidzenko, S. K. Krikalev, W. Shepherd, A. I. Ivanov, M. Roth, H. Binnenbruck, J. Goree, and Y. P. Semenov. PKE-Nefedov: plasma crystal experiments on the International Space Station. *New J. Phys.*, 5:33, 2003.

[44] M. Cavarroc, M. Mikikian, Y. Tessier, and L. Boufendi. Successive generations of dust in complex plasmas: A cyclic phenomenon in the void region. *Phys. Rev. Lett.*, 100:045001, 2008.

[45] S. Hong and J. Winter. Size dependence of optical properties and internal structure of plasma grown carbonaceous nanoparticles studied by in situ Rayleigh-Mie scattering ellipsometry. *J. Appl. Phys.*, 100:064303, 2006.

[46] L. Boufendi, M. -C. Jouanny, E. Kovacevic, J. Berndt and M. Mikikian. Dusty plasma for nanotechnology. *J. Phys. D: Appl. Phys.*, 44:174035, 2011.

[47] M. Cavarroc, M. C. Jouanny, K. Radouane, M. Mikikian, and L. Boufendi. Self-excited instability occurring during the nanoparticle formation in an Ar - SiH_4 low pressure radio frequency plasma. *J. Appl. Phys.*, 99:064301, 2006.